Development of Thick $Sc_{0.2}Al_{0.8}N$ Film for MEMS Application

Jaibir Sharma, Daniel Ssu-Han Chen, Yong Shun Teo, Peng Liu
Institute of Microelectronics (IME), Agency for Science, Technology, and Research (A*STAR),
Singapore 138632, Republic of Singapore
2 Fusionopolis Way, Singapore 138634
sharmaj@ime.a-star.edu.sg

Abstract

The integration of new material for any device as a structural and packaging material invariably requires a lot of development for deposition, etching, and cleaning etc. This procedure becomes more critical with the increase in material thickness. This work reports the development of a 1.3 µm thick $Sc_{0.2}Al_{0.8}N$ film deposition by sputtering. The film was optimized to reduce the number of Abnormally Oriented Grains (AOG) in the film by using pre-treatment conditions before the deposition of the film. The results show a tremendous reduction in the number of AOG. The optimized 1.3 µm thick $Sc_{0.2}Al_{0.8}N$ film is used in the optimization of the dry etching process using the ICP technique with photoresist as a mask on an 8-inch wafer. The etch recipe was optimized for focusing on reduced etch time and better selectivity with photoresist. The developed recipes were successfully applied to fabricate the GHZ range transducers with molybdenum (Mo) as a routing layer. Subsequent electrical measurements on the fabricated transducer devices confirmed the successful integration of 1.3 µm thick $Sc_{0.2}Al_{0.8}N$, demonstrating its potential for MEMS applications.

I. Introduction

In the present decade, there is an exploration of many types of piezoelectric MEMS and NEMS device for various application such as actuators [1], transducers [2], resonators [3], radio frequency (RF) MEMS switch [4], RF MEMS filters [5], PMUT [6] etc. AlN, PZT, ZnO, and PVDF are piezoelectric materials that have been used by various groups for the realization of these devices. Out of these materials, AlN [7] is a commonly used material due to its simplicity in process integration, low-temperature PVD deposition, tunable stress as per desire during PVD deposition, volatility of its byproducts during RIE etching using Cl_2/BCl_3 chemistry, and its CMOS compatibility. In addition, introducing scandium (Sc) doping in AlN will enable ferroelectric properties ($Sc_xAl_{1-x}N$: for x is $0<x<40$) and possess an increase in its piezoelectric constant with doping concentration. The incremental enhancement of the piezoelectric constant with a higher concentration of Sc in AlN results in a higher electromechanical coupling of the piezoelectric device. One of the research groups recently demonstrated an electromechanical coupling coefficient of more than 20% for 15% Sc concentration [8]. The demonstration of a higher coupling coefficient of scandium-doped AlN makes it a suitable material for the fabrication of wideband acoustic and high-frequency devices. However, the increase in the doping concentration of scandium invariably impacts the deposition and dry etching of AlN. The involvement of the Sc during AlN deposition results in the formation of cone-shaped islands on the deposited thin film. These cone-shaped islands are uncontrolled growth of abnormal oriented grains (AOG) of $Sc_xAl_{1-x}N$ [9]. The size and number of these AOG in the deposited film depend upon the substrate, deposition conditions, and thickness of the deposited film. This issue of AOG formation makes it pensive for thicker $Sc_xAl_{1-x}N$ deposited film. The average diameter size of AOG can vary from 200 nm to 800 nm [10] depending on deposition conditions and thickness of the film. The presence of these AOG subsequently results in undesirable surface roughness in the deposited thin film which negatively impacts the device performance [10,11]. Another impact of this AOG presence happens in the dry etching of the film during patterning for the via and structural layer. Dry etching of such non-uniform $Sc_xAl_{1-x}N$ film requires a considerable amount of over-etching to clear the AOG region which results in a substantial amount of over-etching of the bottom layer, typically molybdenum electrodes, and hence failure of the fabricated device. This problem worsens with the increment of $Sc_xAl_{1-x}N$ film thickness. The etching issue of these non-uniform $Sc_xAl_{1-x}N$ films can be solved by considering wet etching solutions such as 25% TMAH, MIF-319 developer containing 2-5% TMAH and 10-30 % KOH. However, wet etch solutions cannot be used for the fabrication of miniaturized devices due to their isotropic lateral etching nature. The above discussion clarifies that there is a real requirement to reduce the AOG in $Sc_xAl_{1-x}N$ film.

Another issue with $Sc_xAl_{1-x}N$ film is observed during its dry etching. It is found that $Sc_xAl_{1-x}N$ dry etching is more challenging and time-consuming compared to etching AlN, even with the same etch recipe. As the Sc percentage in AlN increases, the etching of $Sc_xAl_{1-x}N$ becomes more difficult. The extended etch timing affects the selection of the mask type and its thickness for etching the $Sc_xAl_{1-x}N$ film, potentially impacting the minimum achievable critical dimension (CD) of these materials. Furthermore, increment in the $Sc_xAl_{1-x}N$ film thickness aggravates the above issues of extended etch time, proper selection of etch mask, and its thickness. Fig. 1 depicts the etching process of the $Sc_xAl_{1-x}N$ film, highlighting the use of a photoresist (PR) as the preferred mask for etching. The thickness of PR tends to increase with the thickness of $Sc_xAl_{1-x}N$.

Different dry etching techniques such as RIE, ICP, IBE and RIBE have been explored by various groups for etching different doping percentages of Sc in AlN which is well summarized by Shifat et al. [8]. Luo et al. [12] reported etching of 6% doped ScAlN using the ICP technique with photoresist (PR) as an etch mask to achieve an etch rate close to 230 nm/min with a side wall angle of 84°.

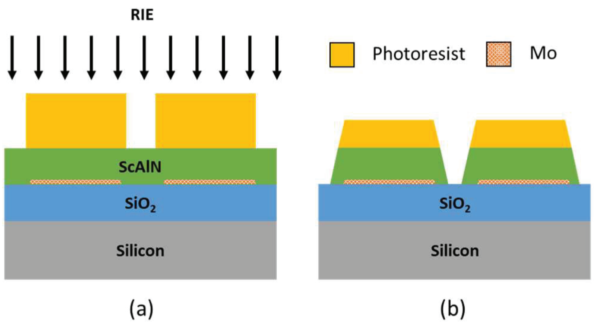

Fig. 1. Illustration of the etching process: (a) pattern photoresist as etch mask; (b) during the etching process, the PR will get consumed laterally, resulting in a tapered sidewall.

Wang et al [13] realized pMUT with 15 % doped ScAlN by RIE dry etching using PR as a mask and reported an etch rate of 160 nm/min. Shao et al. [14] realized a resonator with 22% doped ScAlN using the ICP technique with oxide as a mask and reported an etch rate of 130 nm/min. However, as discussed above, PR is preferred as a mask for etching ScAlN to avoid the overburden of depositing and etching the extra hard mask before etching ScAlN. This work was concentrated on the following tasks:

1. Optimization of pre-treatment condition on the wafer surface for reducing AOG formation in a 1.3 µm thick $Sc_{0.2}Al_{0.8}N$ film, compared to that without.
2. The optimized deposition film was used for optimizing the dry etching using the ICP technique with 4.5 µm thick PR as a mask. This study focuses on optimizing the etch recipe to reduce etch timing specifically for a 1.3 µm thick $Sc_{0.2}Al_{0.8}N$ film.
3. Finally, the resulting optimized recipe is utilized in fabricating high frequency (GHz) acoustic transducers, including those with diameters smaller than 2 µm.

II. Process flow and fabrication of transducer

The optimization of recipes and fabrication of the MEMS transducers was performed on 8-inch silicon (Si) <100> wafers. The deposition recipe was optimized by using different prior treatment conditions to reduce the size and number of AOG in the 1.3 µm $Sc_{0.2}Al_{0.8}N$ film. The optimized recipe was utilized to fabricate the high frequency GHz transducer. Fig. 2 shows the process flow used to fabricate the MEMS transducer. Fig. 2(a) shows the cross-section illustration after deposition and patterning of the 0.3 µm Mo as the bottom electrode (BE). It should be noted here that $Sc_{0.2}Al_{0.8}N$ dry etching does not have a good selectivity on Mo. Even though the dry etch recipe was optimized for good selectivity to preserve bottom Mo, still it is not high enough to preserve the thin Mo layer. So, to realize the integration of 1.3 µm thick $Sc_{0.2}Al_{0.8}N$ film on bottom Mo, 0.3 µm thick bottom Mo was considered to preserve bottom Mo during etching of $Sc_{0.2}Al_{0.8}N$ film on Mo for patterning the via and structural layers. Next, 1.3 µm thick $Sc_{0.2}Al_{0.8}N$ was deposited using an optimized recipe (for low AOG) with the SPTS PVD tool. The 1.3 µm thick $Sc_{0.2}Al_{0.8}N$ film was patterned to form via and structure layer with 4.5 µm thick PR. This is followed by dry etching of $Sc_{0.2}Al_{0.8}N$ using an optimized etch recipe. Fig. 2(b) shows the illustration after via and structural layer patterning. After performing via and structural layer pattern, the Mo as top electrode (TE) was deposited and patterned as depicted in Fig. 2(c). Next, a 3.5 µm thick oxide layer was deposited, and oxide CMP was performed to planarize the surface. Left-out oxide on the Mo was in the range of 0.4 µm to 0.6 µm. Fig. 2(d) illustrates after oxide CMP. Next, the pad area is patterned in the oxide as shown in Fig. 2(e). Finally, gold (Au) was deposited and patterned to define the Au pad.

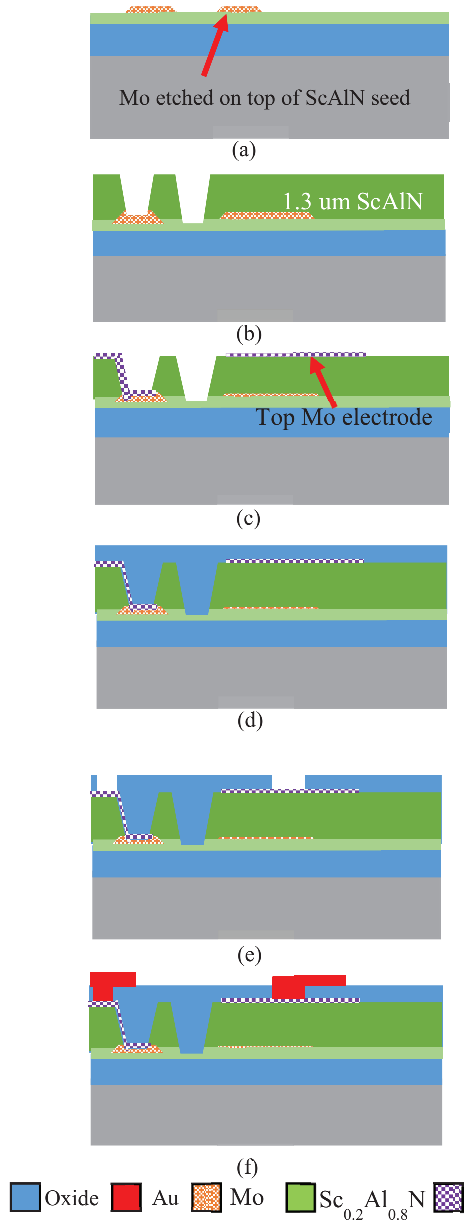

Fig. 2. Process flow to fabricate the GHz range MEMS transducer after: (a) BE Mo patterning, (b) via and structural patterning in $Sc_{0.2}Al_{0.8}N$, (c) TE Mo patterning, (d) after 3.5 µm oxide deposition and CMP to keep 0.5 µm oxide, (e) pad area pattering in oxide, (f) patterning Au pad.

III. Results and discussion

a. Optimization of deposition condition for 1.3 µm thick $Sc_{0.2}Al_{0.8}N$

Fig. 3 shows the top SEM image for the 1.3 µm thick $Sc_{0.2}Al_{0.8}N$ deposited film. The film was deposited by pre-treating the wafer using two different conditions as well as without. The focus of view (FOV) for the SEM images is 10 µm. Fig. 3(a) shows the SEM image for the 1.3 µm thick $Sc_{0.2}Al_{0.8}N$ film deposited without any prior treatment on the wafer. It is clear from the SEM image that there are large numbers of cone-shaped AOG formations taking place on the whole 8-inch wafer. Integration for this type of non-uniform film may be difficult for device fabrication as there can be a complete loss of BE during clearing of ScAlN everywhere on the wafer including the AOG area. At the same time, the fabricated device performance may deviate from its actual designed value, and it may not be reliable. Fig. 3(b) shows the SEM image of the 1.3 µm thick $Sc_{0.2}Al_{0.8}N$ where the wafer was treated with condition 1 prior to deposition of ScAlN. The SEM image shows a reduction in the number of AOG in comparison to the untreated one even though the size of cone-shaped AOG results remain similar. Still, this type of film is difficult to integrate for the fabrication of the device. Furthermore, the condition was improved to get better ScAlN film. Fig. 3(c) shows the SEM image for the 1.3 µm thick $Sc_{0.2}Al_{0.8}N$ film where the wafer was treated with condition 2 prior to ScAlN deposition. It is clear from the SEM image that the number of unwanted AOG is reduced drastically. This film was used to optimize the dry etching of 1.3 µm thick $Sc_{0.2}Al_{0.8}N$ film with 4.5 µm thick photoresist as a mask. Later, these recipes were used for the fabrication of GHz range transducers.

b. Optimization of dry etching for 1.3 µm thick $Sc_{0.2}Al_{0.8}N$

The optimized 1.3 µm thick $Sc_{0.2}Al_{0.8}N$ film is used for developing a high etch rate and high selectivity recipe with respect to the PR mask. A 4.5 µm thick PR mask was considered for etching 1.3 µm thick $Sc_{0.2}Al_{0.8}N$ film. Fig. 4(a) shows the SEM image of the sample after etching 1.3 µm thick $Sc_{0.2}Al_{0.8}N$ film using dry etch recipe 1. It can be observed from the SEM image that PR was almost depleted during the etching of 1.3 µm thick $Sc_{0.2}Al_{0.8}N$ film. The total etch time for the film was 575 sec which results in an etch rate of 136 nm/min. To achieve a higher etch rate and better selectivity of the $Sc_{0.2}Al_{0.8}N$ with respect to PR, high power etch recipe was used. Fig. 4(b) shows the SEM image of the sample after etching the 1.3 µm thick $Sc_{0.2}Al_{0.8}N$ film using a high-power etch recipe before PR stripping. It is clear from the image that there is still room for etching thicker $Sc_{0.2}Al_{0.8}N$ film than 1.3 µm. Even smaller transducers of 2 µm diameter were left with a PR mask on the top of the pattern (Fig. 4(c)). The 1.3 µm $Sc_{0.2}Al_{0.8}N$ film etch was completed in 480 sec resulting in an etch rate of ~163 nm/min. Due to the recessing of the PR in the lateral direction during etching, the $Sc_{0.2}Al_{0.8}N$ sidewall resulted in tapering and the tapered angle was measured to be 50° as shown in Fig. 5(a). Even though this recipe results in tapering during the ScAlN etch, still it was useful in patterning a 1.7 µm wide trench for the 1.3 µm thick $Sc_{0.2}Al_{0.8}N$ film as shown in Fig. 5(b). Fig. 5(b) shows the SEM image for a 2 µm wide small transducer which is successfully etched using this recipe.

c. High frequency transducer fabrication

After the optimization of the deposition and etch recipe for ScAlN, this recipe was utilized in the fabrication of the GHz transducers by following the process flow discussed in section II. Fig. 6(a) and (b) shows the optical and SEM image, respectively, for the MEMS device fabricated using the optimized recipe.

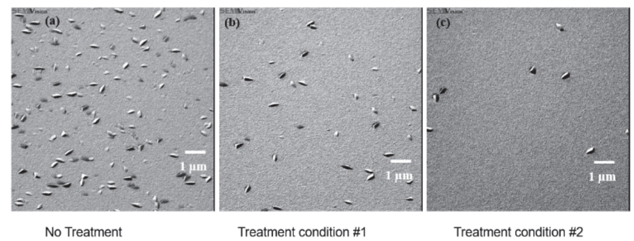

Fig. 3. Top SEM image for the samples after $Sc_{0.2}Al_{0.8}N$ deposition: (a) without prior treatment, (b) with prior treatment condition 1, (c) with prior treatment condition 2.

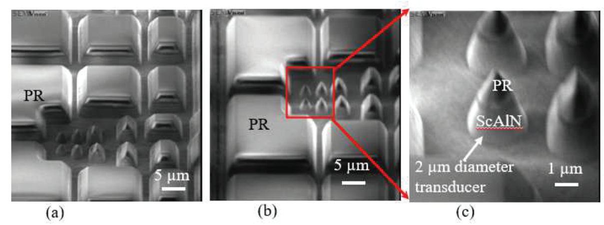

Fig. 4. Top SEM image for the samples after etching 1.3 µm thick $Sc_{0.2}Al_{0.8}N$ without PR stripping: (a) with recipe 1, (b) with modified high-power etch recipe 2, (c) enlarge view of (b) to highlight left-out PR on a 2 µm diameter transducer.

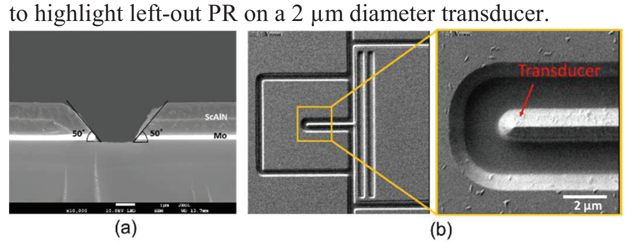

Fig. 5. (a) Cross-section SEM image showing the sidewall profile after etching; (b) ScAlN transducer with 1.7 µm CD.

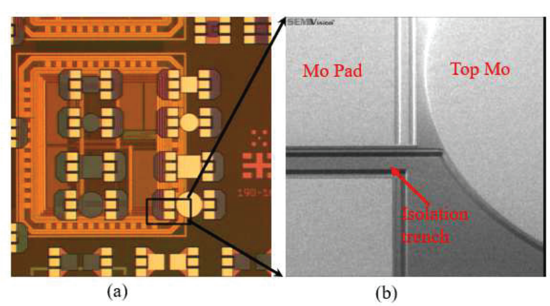

Fig. 6. (a) Optical image for one of the fabricated transducer devices, (b) top SEM image of the transducer device after Mo TE patterning.

d. Electrical characterization of GHz transducer

Preliminary vector network analyzer (VNA) measurements were performed to validate the fabricated transducers functionality. The device measured was a set of transducers with a solidly mounted bulk acoustic wave resonator (BAW-SMR) configuration. The inset figure in Fig. 7(a) shows the optical image of the device under test (DUT). The left channel (CH1) is a large transducer surrounding an island of another smaller transducer connected to another channel (CH2). The S-parameters were measured using the two-port network configuration. The input return loss, S_{11}, shows the device peak resonance around 1.88 GHz with spacing of the parallel resonant frequency (SPRF) of 5.73 MHz (Fig. 7(a)). Alternatively, the insertion loss, S_{21}, is found to have the same resonant peak and SPRF (Fig. 7(b)).

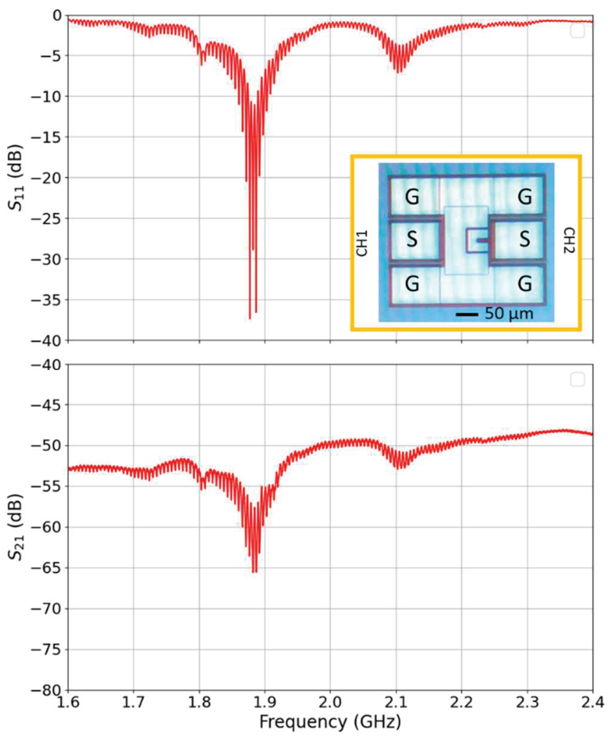

Fig. 7. S-parameter measurements with left transducer connected to CH1 and right transducer island connected to CH2: (a) S_{11} (b) S_{21}.

Conclusions

ScAlN, a CMOS-compatible material, possesses exceptional mechanical and electrical properties that render it suitable for diverse MEMS applications. Its utilization in MEMS devices contributes to enhanced performance, miniaturization, and functionality. Achieving higher concentrations of Sc-doped AlN while reducing the occurrence of abnormally oriented grains (AOGs) is crucial not only for the device performance perspective but also for simplifying device integration processes. In this work, 1.3 µm thick Sc-doped AlN film was optimized by focusing on the reduction of the number of AOG. Further, the optimized recipe was used to optimize the dry etching recipe using 4.5 µm thick PR as a mask layer. The 1.7 µm wide trench was successfully etched and a high etch rate of ~163 nm/min was achieved. After etch completion of 1.3 µm thick $Sc_{0.2}Al_{0.8}N$, approximately 50 % PR mask was left out on the larger patterns which shows that the developed recipe has good selectivity and is capable of etching thicker $Sc_{0.2}Al_{0.8}N$ film using 4.5 µm thick PR Mask. The optimized recipes were successfully utilized in the fabrication of the GHz range MEMS transducer. Even a 2 µm diameter transducer is also fabricated using the developed etch recipe. These recipes can be used for the fabrication of other MEMS devices.

Acknowledgments

This research is supported by A*STAR RIE2020 Advanced Manufacturing and Engineering Programmatic under the "Ultrasonic Wavefront Computing" grant (A19E8b0102).

References

1. H. J. Quenzera , U. Drechslerb , A. Sebastianb , S. Marauskaa , B. Wagnera , M. Despontb, "*Fabrication of conducting AFM cantilevers with AlN-based piezoelectric actuators*" Procedia Engineering 25 (2011) 665 – 668.
2. Cyril Baby Karuthedath, Abhilash Thanniyil Sebastian, Jaakko Saarilahti, Teuvo Sillanpaa and Tuomas Pensala, "*Design and Fabrication of Aluminum Nitride Piezoelectric Micromachined Ultrasonic Transducers for Air Flow Measurements*" IEEE International Ultrasonics Symposium (IUS), 06-09 October 2019, Glasgow, UK.
3. M. Rinaldi, C. Zuniga, C. Zuo and G. Piazza, "*ULTRA-THIN SUPER HIGH FREQUENCY TWO-PORT ALN CONTOUR-MODE RESONATORS AND FILTERS*" Transducers 2009, Denver, CO, USA, June 21-25, 2009, pp 577-580.
4. R. R. Benoit, R. Q. Rudy, J. S. Pulskamp, R. G. Polcawich and S.S. Bedair *"Advanced in Piezoelectric PZT-based RFMEMS components and systemes*" Journal of Microelectronics and Microengineering, Vol 27(2017), 083002
5. Roman Lanz and Paul Muralt, "*Bandpass Filters for 8 GHz Using Solidly Mounted Bulk Acoustic Wave Resonators*" IEEE Transactions on Ultrasonics, Ferroelectrics, and Frequency Control, vol. 52, no. 6, June 2005, pp 936-945.
6. Choong, D. S. W., Chen, D. S.-H., Goh, D. J., Liu, J., Ghosh, S., Koh, Y., Sharma, J., Merugu, S., Quaglia, F., Ferrera, M., Savoia, A. S., & Ng, E. J. , "Silicon-On-Nothing ScAlN pMUTs" 2021 IEEE International Ultrasonics Symposium (IUS). https://doi.org/10.1109/ius52206.2021.9593461.
7. Jaibir Sharma, Sanchitha Fernando and Wee Ming Tan, "Integration of AlN with molybdenum electrodes and sacrificial amorphous silicon release using XeF2" *J. Micromech. Microeng.* 24 035019
8. A. S. M. Zadid Shifat , Isaac Stricklin , Ravi Kiran Chityala , Arjun Aryal , Giovanni Esteves, Aleem Siddiqui and Tito Busani,"*Vertical Etching of Scandium Aluminum Nitride Thin Films using TMAH Solution"* Nanomaterials 2023, 13, 274.
9. Zichen Tang, Giovanni Esteves, Jeffrey Zheng and Roy H. Olsson III, "Vertical and Lateral Etch Survey of Ferroelectric $AlN/Al_{1-x}Sc_xN$ in Aqueous KOH Solutions" Micromachines 2022, 13, 1066.
10. Liu, Chen, et al. "Evaluation of the impact of abnormal grains on the performance of Sc0. 15Al0. 85N-based BAW

resonators and filters." *Journal of Micromechanics and Microengineering*, Vol 32., No 3 (2022): 034002.

11. Sandu, Cosmin Silviu, et al. "Abnormal grain growth in AlScN thin films induced by complexion formation at crystallite interfaces." *physica status solidi* (a), Vol. 216, No. 2 (2019): 1800569.
12. Luo Z., Shao S., Wu T., "*Optimization of AlN and AlScN Film ICP Etching*" IEEE 34th International Conference on Micro Electro Mechanical Systems (MEMS), Gainesville, FL, USA, 25–29 January 2021; pp. 638–641.
13. Wang Q., Lu Y., Mishin S., Oshmyansky Y., Horsley D.A., "*Design, Fabrication, and Characterization of Scandium Aluminum Nitride-Based Piezoelectric Micromachined Ultrasonic Transducers*." J. Microelectromech. Syst. 2017, 26, 1132–1139.
14. Shao S., Luo Z., Lu Y., Mazzalai A., Tosi C., Wu T., "*High Quality Co-Sputtering AlScN Thin Films for Piezoelectric Lamb-Wave Resonators"* J. Microelectromech. Syst. 2022, 31, 328–337.